SYMPOSIUM

Passive Robotic Models of Propulsion by the Bodies and Caudal Fins of Fish

George V. Lauder,[1],* Brooke Flammang* and Silas Alben[†]

*Museum of Comparative Zoology, Harvard University, Cambridge, MA 02138, USA; [†]School of Mathematics, Georgia Institute of Technology, Atlanta, GA 30332, USA

[1]E-mail: glauder@oeb.harvard.edu

Synopsis Considerable progress in understanding the dynamics of fish locomotion has been made through studies of live fishes and by analyzing locomotor kinematics, muscle activity, and fluid dynamics. Studies of live fishes are limited, however, in their ability to control for parameters such as length, flexural stiffness, and kinematics. Keeping one of these factors constant while altering others in a repeatable manner is typically not possible, and it is difficult to make critical measurements such as locomotor forces and torques on live, freely-swimming fishes. In this article, we discuss the use of simple robotic models of flexing fish bodies during self-propulsion. Flexible plastic foils were actuated at the leading edge in a heave and/or pitch motion using a robotic flapping controller that allowed moving foils to swim at their self-propelled speed. We report unexpected non-linear effects of changing the length and stiffness of the foil, and analyze the effect of changing the shape of the trailing edge on self-propelled swimming speed and kinematics. We also quantify the structure of the wake behind swimming foils with volumetric particle image velocimetry, and describe the effect of flexible heterocercal and homocercal tail shapes on flow patterns in the wake. One key advantage of the considerable degree of control afforded by robotic devices and the use of simplified geometries is the facilitation of mathematical analyses and computational models, as illustrated by the application of an inviscid computational model to propulsion by a flapping foil. This model, coupled with experimental data, demonstrates an interesting resonance phenomenon in which swimming speed varies with foil length in an oscillatory manner. Small changes in length can have dramatic effects on swimming speed, and this relationship changes with flexural stiffness of the swimming foil.

Introduction

The study of structure and function in different species is a hallmark of comparative biology. Documenting how morphology and physiology vary both among closely related species and across broader phylogenetic scales is perhaps the most common approach used in the field of functional morphology and evolutionary biomechanics. This comparative approach has both strong theoretical underpinnings (Feder et al. 1987; Harvey and Pagel 1991; Garland and Adolph 1994; Vogel 2003; Felsenstein 2004) and a wealth of experimental techniques that can be utilized to better understand differences among species in their structure and function (Wainwright et al. 1976; Biewener 1992).

The comparative approach, however, has significant limitations. Chief among these is the inability to study the effect on performance of individual traits while keeping all other aspects of morphology and physiology constant. It is certainly possible to reconstruct evolutionary patterns of morphology and physiology, but many correlated changes occur in animals' structure and function that make isolating individual traits impossible. For example, one noteworthy trend in the evolution of fishes is the change in tail structure from the morphologically asymmetrical heterocercal tail shape seen in sharks and other basal ray-finned fishes to the externally symmetrical homocercal tail of most teleost fishes (Kardong 1998; Lauder 2000; Liem et al. 2001;

Lauder 2006). Using the comparative method, it is not possible to isolate the effect of tail shape alone on locomotor performance, while keeping all other traits constant. Sharks differ from bony fishes in so many ways that it is not particularly useful to compare species in these two groups if the specific goal is to understand the effect of tail shape on swimming performance.

Additional constraints on the comparative method include the frequent lack of suitable variation among extant species, so that certain hypotheses simply cannot be tested. If we wished to study the effect of body length on locomotor performance in zebrafish, we would not be able to conduct a comparative study of live individuals over a size range that extends up to 1 m. Of course, many other changes in zebrafish's anatomy and physiology occur as body length changes, so once again the limitations of comparing animals restrict our ability to isolate effects of the trait of interest.

Two approaches that allow the isolation of individual traits and that are increasingly available to comparative biologists are (1) the construction of robotic devices, and (2) the use of computational models. Robotic devices provide a physical model of animal function and allow individual traits to be altered while controlling all others (Koditschek et al. 2004; Koehl et al. 2011; Lauder et al. 2011a; Long 2012). At the same time, many quantities of interest in assessing locomotor performance such as measurements of force and power output can be made which are difficult to achieve on freely-moving animals. In addition, computational modeling is a powerful method that offers the ability to explore a large parameter space and isolate individual traits of interest (e.g., Mittal 2004; Alben 2009a, 2010; Borazjani and Sotiropoulos 2010; Dong et al. 2012). For example, in a computational model of swimming fishes it is relatively easy to alter body stiffness and length, a manipulation that ranges from difficult (Long et al. 1996) to impossible with live animals.

In this article, our goals are (1) to use a simple robotic model of swimming fishes to explore a number of features of functional design in fishes, including the effects of body length, stiffness, and tail shape on locomotor performance, and (2) to apply a computational model that incorporates key features of the robotic system to explore in detail the relationship between body length and swimming performance. We show that even simple traits such as body length or stiffness can have unexpected non-linear effects on swimming, and we suggest that complementary robotic and computational approaches are an important adjunct to traditional comparative methods for the study of organismal function.

Robotic and computational methods

We have implemented a simple robotic model of the bending body and traveling wave used during steady rectilinear swimming by fishes. This robotic system, discussed in more detail elsewhere (Lauder et al. 2007, 2011a, 2011b), uses flexible plastic foils (of similar area and aspect ratio to moderate-sized fishes) that are driven at their leading edge by a computer-controlled robotic flapper. These foils span the range of measured flexural stiffnesses of passive fish bodies (McHenry et al. 1995; Long 1998; Long et al. 2002), and provide an excellent model for body bending during undulatory locomotion by fish. The robotic mechanism controls both heave and pitch motions of the foil's leading edge, and these movements generate a traveling wave that produces forces and torques measured on the shaft holding the flexible plastic foil.

These plastic foils swim in a recirculating flow tank (with a cross-sectional area of 19 x 19 cm, and a length of 50 cm parallel to the direction of flow), and exhibit key characteristics of undulatory locomotion in freely-swimming fishes (Lauder and Tytell 2006): a wave of bending that travels from anterior to posterior, Strouhal numbers that range from 0.2 to 0.4, and Reynolds numbers of 10,000–50,000 (based on foil length). Tests of foil swimming are thus done at-scale. These moving foils are designed to reflect the thrust generating region of swimming fishes, which for low to moderate swimming speeds is the posterior half of the body in most species. Beat amplitudes of the foil tail are thus not directly comparable to those of swimming fishes relative to total length. Nonetheless, Strouhal numbers of swimming foils and live fishes are comparable, which indicates that the dynamics of undulatory locomotion in fishes are well captured by the swimming foil system (Triantafyllou and Triantafyllou 1995).

The design of the robotic flapper includes a low-friction air-carriage that allows the foil to self-propel and to swim in place against a current that is tuned to the mean swimming speed of the foil. Changing the motion parameters, materials, and shape of the foil results in changes in self-propelled swimming speed, which are measured using a custom LabView program. Studying self-propelling objects is critical to understanding the dynamics of locomotion, as emphasized elsewhere (Schultz and

Webb 2002; Lauder et al. 2007, 2011a; Borazjani and Sotiropoulos 2010; Tytell et al. 2010). When swimming bodies self-propel, thrust and drag forces are balanced over a tail beat cycle. If a swimming object is towed at a different speed, thrust and drag forces will not be balanced and the wake generated by the swimming object can be quite different from that of a self-propelled swimmer (Lauder et al. 2011a). One advantage of studying the locomotion of flexible plastic foils is that alterations in length and in the shape of the trailing edge can be easily accomplished. Furthermore, by changing the material in the foil it is also a simple matter to alter the flexural stiffness of the foil and to study the effect of stiffness on swimming performance.

In order to understand the mechanical and hydrodynamic basis of the foil's swimming performance, it is important to quantify both the three-dimensional motion of the foil and the wake produced during swimming. Three-dimensional movements of swimming foils were measured using three synchronized Photron PCI-1024 digital video cameras, and a direct linear transformation (DLT) calibration was implemented to provide accurate x, y, and z coordinates of points on the swimming foils (Standen and Lauder 2005; Hedrick 2008; Flammang and Lauder 2009). Volumetric measurement of the pattern of flow in the foil's wake was accomplished using the TSI V3V volumetric flow visualization system (details provided in Flammang et al. [2011a, 2011b]).

Our computational modeling of foil swimming used the inviscid analytical approach developed by Alben et al. (2008, 2009b, 2012). This computational approach is two-dimensional and uses measurements of the foil's length and flexural stiffness to compute self-propelled swimming speeds and patterns of flow in the wake while accounting for structure-fluid interactions.

Results

Effects of length on swimming speed

One of the simplest possible parameters that could be examined for effects on swimming performance is length. How do alterations in the length alone of a flexible swimming object affect propulsion? For studies of live fishes, one could examine changes in propulsion through ontogeny as fishes grow and increase in length, but such comparisons are confounded by changes in mass, body shape, muscle and respiratory physiology, for example, which all change in conjunction with length as fishes grow. A robotic approach allows study of the effects of simple alterations in length of the foil on swimming speed and provides a direct focus on the dynamics of propulsion alone.

Figure 1 plots experimental data from the robotic flapper that demonstrate unexpected non-linear effects of foil length on self-propelled swimming speed. For example, the yellow plot (foil stiffness =
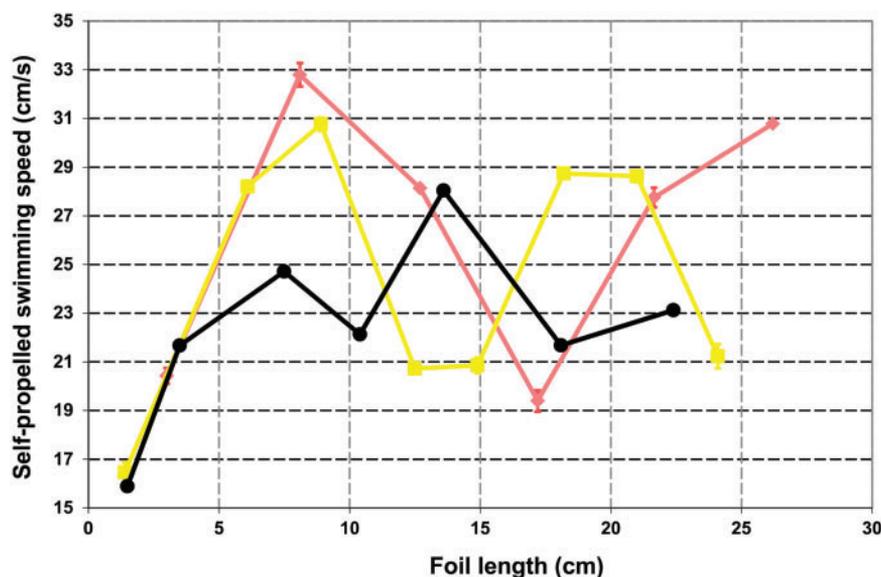
Fig. 1 Experimental data measuring self-propelled swimming speed versus foil length for flexible foils of three different flexural stiffnesses. Foils were actuated with ± 1.0 cm heave amplitude at the leading edge at a frequency of 2 Hz, with no pitch motion. Error bars of ± 1 SE are plotted for each point, but some error bars are obscured by the symbols. Note that certain stiffnesses of foils (yellow plot) show multiple peaks in swimming speed as length of the foil changes, and that even relatively small changes in length can have substantial effects on swimming speed. Foil flexural stiffnesses: coral color = 4.9×10^{-3} Nm^2; yellow = 9.9×10^{-4} Nm^2; black = 0.32×10^{-4} Nm^2. (Reference to color applies to online version, not to printed black and white version.)

9.9 × 10^{-4} Nm^2) shows two distinct peaks and troughs over the range of foil lengths studied. A change of only 5 cm in length caused a decrease in swimming speed of ~33%, but a further increase in foil length produced a 50% increase in swimming speed. Swimming by foils of other stiffness also showed significant non-linear changes in speed as the length of the foil was increased: Prominent peaks and valleys were evident in swimming speed (Fig. 1). These experimental data demonstrate that there is no simple relationship between swimming speed and length or stiffness of the foils, and that these two parameters interact in a complex manner. Furthermore, the experimental data showing multiple peaks in swimming speed suggest that the flexible foils are experiencing a resonance phenomenon in which certain lengths interact with the moving fluid in a manner that enhances propulsion, while other lengths interact in a negative manner that decreases swimming speed.

To explore a broader range of lengths and more precisely document this resonance phenomenon than is possible from experimental data alone, we used a two-dimensional inviscid analytical model of swimming foils to calculate self-propelled swimming speeds for a wide range of lengths and for foils of two flexural stiffnesses (Fig. 2). The range of foil lengths that we can study experimentally is limited by the size of our flow tank, and small differences in self-propelled speed are difficult to measure accurately. An inviscid computational approach can be used to explore a much larger parameter space than is possible experimentally. Comparison of the foil shapes during swimming measured both experimentally and computed showed an excellent match (Fig. 2A and B). Furthermore, the computational model revealed a distinct resonance pattern in which swimming speed showed multiple sharp peaks and valleys as length increased, for foils of both studied stiffnesses (Fig. 2C and D). These results confirm that even small changes in length of foils can have dramatic effects on swimming speed, and show that interpreting differences in swimming performance among flexible self-propelling bodies requires knowledge of both flexural stiffness and length of the object.

Effects of stiffness on swimming speed

Fish species vary in body stiffness and in how the body is moved during swimming, but producing a controlled range of variation in stiffness in a living animal is challenging at best (see Long et al. 1996), and it is thus difficult to understand the effect of body stiffness on propulsion solely from comparisons
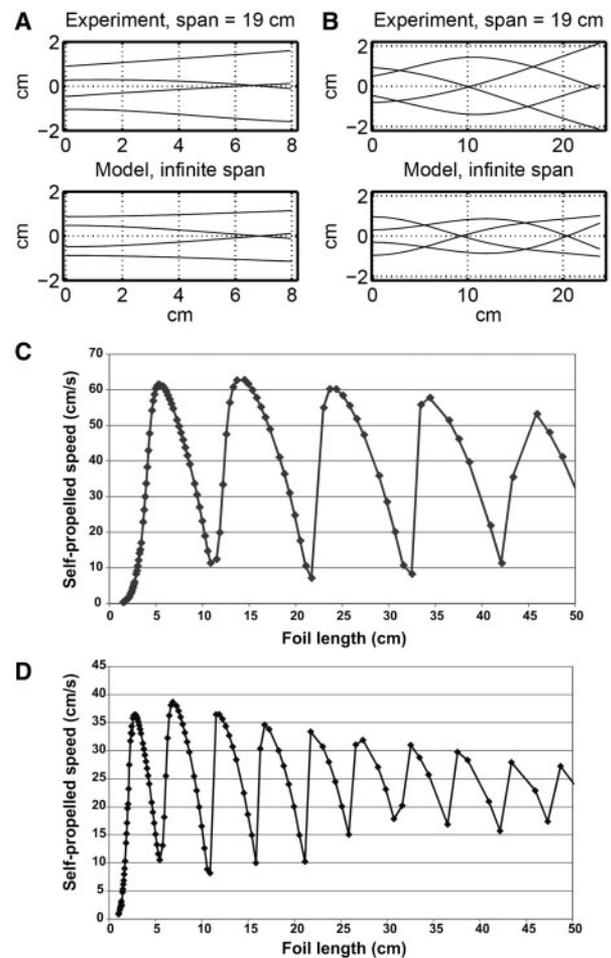

Fig. 2 Results from an inviscid 2D numerical model of propulsion of self-propelled flexible flapping foils (see Alben [2008, 2009b] and Alben et al. 2012 for details of this model) which predicts shape of the foil and the effects of changes in length of the foil on swimming speed. Panels A and B compare experimentally measured and computed midlines of two foils that differ in stiffness, while panels C and D show plots of self-propelled swimming speed versus length for two foils with different stiffnesses. Each point is a separate simulation to calculate the self-propelled swimming speed for that foil. Note the strong resonance peaks that dramatically alter swimming speed as length of the foil changes. Flexural stiffnesses: panel C foil material = 9.9 × 10^{-4} Nm^2; panel D foil material = 3.3 × 10^{-4} Nm^2.

among swimming animals. A robotic approach that involves swimming flexible foils of different stiffnesses and moving the leading edge with different programs of motion allows us to investigate this question in detail.

Figure 3 shows the results of experiments in which self-propelled swimming speed is measured as foils of different flexural stiffness are moved with two different programs of motion at their leading edge: a heave only motion, and heave motion plus pitch movements that impart additional energy into the swimming foil. With the heave-only motion, a
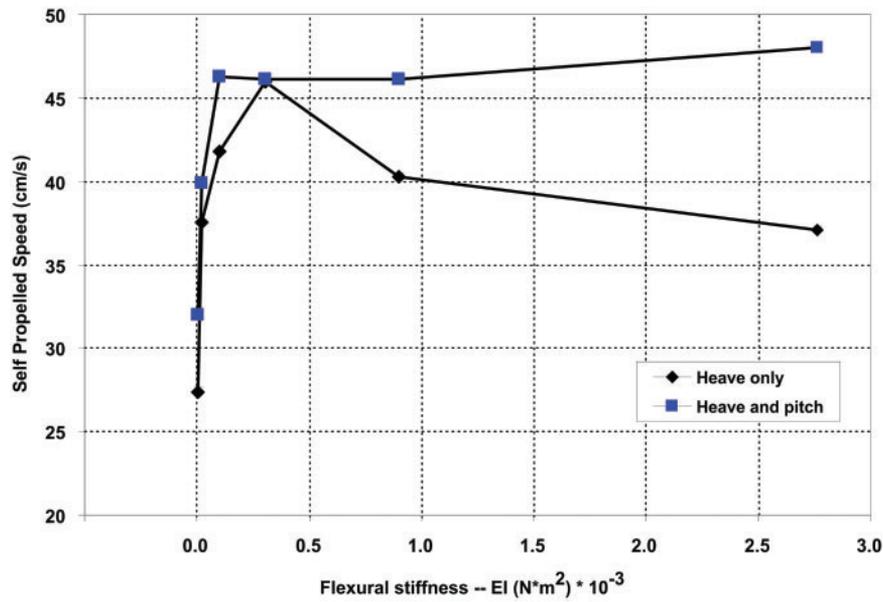
Fig. 3 Self-propelled speed versus flexural stiffness for flexible foils swimming in a recirculating flow tank. Each point represents a different foil. Values plotted are ±1 SE, but error bars are obscured by the symbols. Foils were 19 cm high, 6.8 cm long, and actuated at the leading edge at 1 Hz with ±1.5 cm heave, or ±1.5 cm heave combined with ±20° pitch motion. Foils actuated in heave only show a distinct performance peak, but when pitch motion is added to heave actuation, a broad performance plateau is observed in which swimming speed is relatively independent of flexural stiffness. From Lauder et al. (2011b).
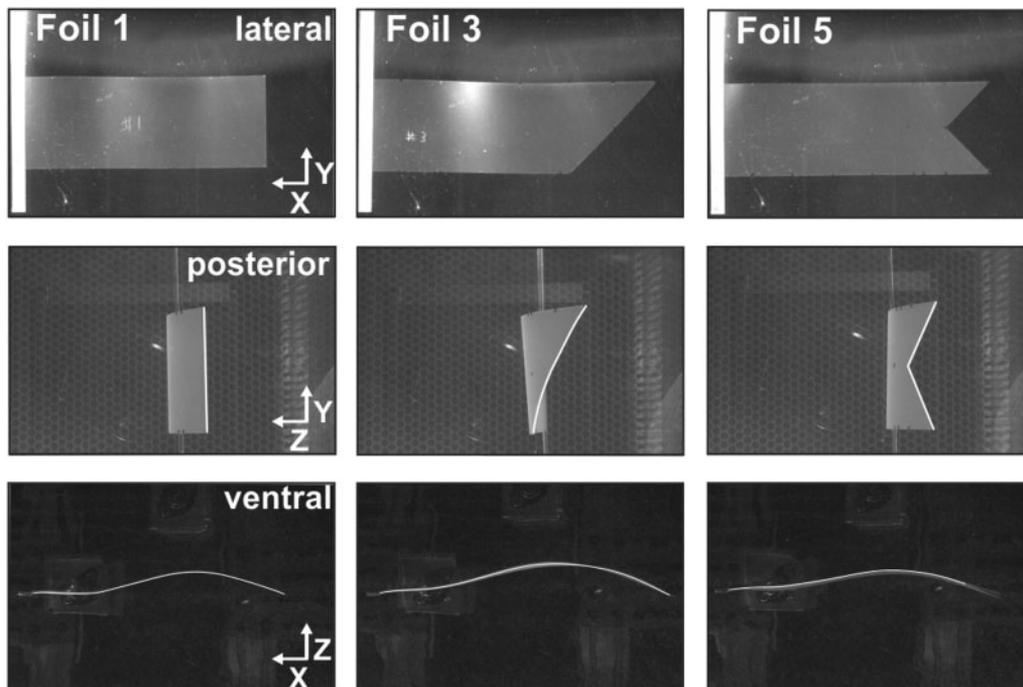

Fig. 4 Propulsion by flexible foils with different trailing edge shapes. Foils have a flexural stiffness of 3.1×10^{-4} Nm^2, and were actuated at the leading edge with ±1 cm heave at 2 Hz (the foil clamping rod is visible on the left side of the top row). Three synchronized high-speed cameras captured lateral, posterior, and ventral views for the foils while they swam at their self-propelled speed. White lines have been added to show the trailing edge in the middle row, and to show the ventral margin in the bottom row (the foil 5 line extends to the tail fork). All foils are shown at the same relative time, when the leading edge is at maximum lateral excursion. Details of foil area, relative shape, and self-propelled swimming speed are given in the text and in the caption to Fig. 6.

distinct peak in performance was observed when swimming speed was maximized at one value of flexural stiffness; but if pitch motion was added to the heave actuation at the leading edge of the foil, this peak disappeared and a broad plateau was observed over which swimming performance was relatively insensitive to changes in flexural stiffness. These results suggest that animals may be able to compensate for changes in stiffness of the body (produced by activation of muscles or from growth and consequent changes in body shape and skeletal features) by changing the way in which propulsive waves are produced, thereby avoiding a decrease in performance at higher stiffnesses. These data also show that the effects of foil stiffness on swimming performance very much depend on how the foil is moved.

Effects of shape of the trailing edge on propulsion

Fish vary considerably in tail shape and yet even simple comparisons among species include so many confounding factors that it is effectively impossible to isolate the effect of tail shape alone on swimming performance. In a robotic flapping-foil system, however, it is easy to alter the shape of the trailing edge of the foil to mimic the shapes of different fish tails and explore the effect of tail shape alone on swimming.

Figure 4 shows the shapes taken by three foils during swimming when powered by the robotic flapper. Foil 1 represents a morphologically symmetrical homocercal fish tail with a vertical trailing edge, foil
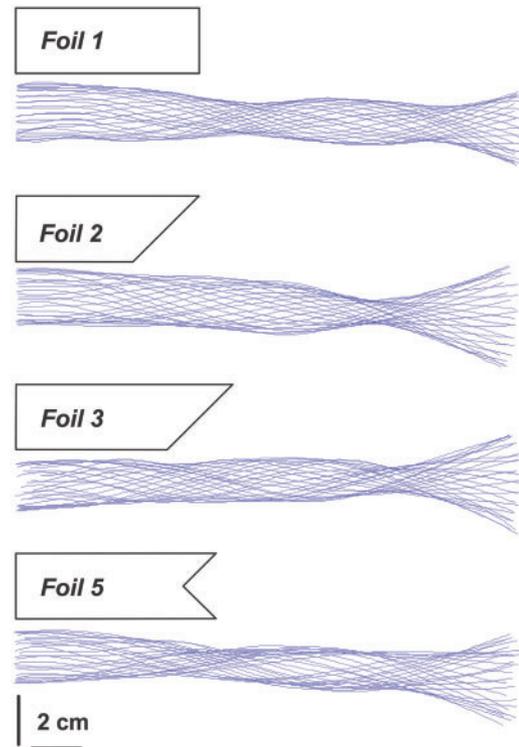
Fig. 5 Midlines of foils as seen in ventral view for self-propelling foils with different shapes of trailing edge. Details of foil area, relative shape, and self-propelled swimming speed are given in the text and in the caption to Fig. 6. Note that rectangular foil 1 displays two nodes which are also seen to a lesser extent in foil 5, but not in the foils with angled trailing edges.
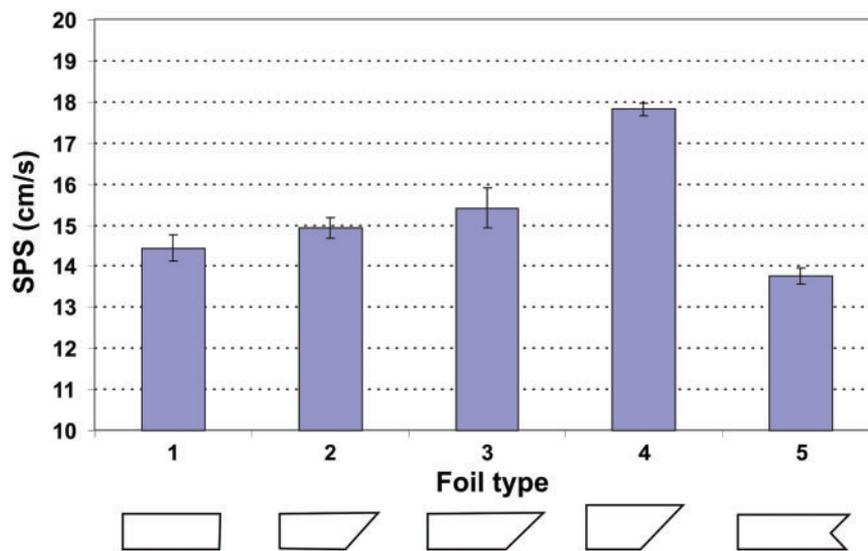
Fig. 6 Self-propelled speeds (SPS) compared for foils (all of material flexural stiffness $= 3.1 \times 10^{-4}$ Nm^2) that differ in shape of the trailing edge and in surface area. Foil-type numbers correspond to those described in Figs 4 and 5. Each foil was actuated at ± 1 cm heave at the leading edge at 2 Hz frequency. Error bars are ± 2 SE. Foils were of different shapes and areas as follows: foil 1 = square trailing edge, area = 131.2 cm^2, dimensions = 6.85 × 19.15 cm; foil 2 = angled trailing edge, same length as foil 1, area = 107.71 cm^2; foil 3 = angled trailing edge, same area as foil 1; foil 4 = angled trailing edge: same length and area as foil 1; foil 5 = forked trailing edge, same area as foil 1. From Lauder et al. (2011a). Statistical analysis of variation in swimming speed is given in the text.

3 has an angled trailing edge reminiscent of a shark's asymmetrical heterocercal tail, and foil 5 has a forked shape with a notch centered between the dorsal and ventral margins. All three of these foils have the same surface area. Although the pattern of bending along the length of each foil was generally similar, the distinct tail shapes did cause some differences in bending (Fig. 5): Foils 1 and 5 had two nodes along their length, while the foils with angled trailing edges only possessed a single node at the base of the tail.

Analysis of the self-propelled speeds of these foils (and an additional one, foil 4, with the same length and area as foil 1) demonstrates four key results (Fig. 6). First, there is highly significant overall variation in swimming performance of these foils (one-way analysis of variance $F = 46.9$; $P < .0001$). Second, the foil with the notched trailing edge (foil 5) had the worst swimming performance, and was significantly slower than all foils except foil 1 (Tukey–Kramer Honestly Significant Difference post hoc test). Third, the foils with the angled (heterocercal) trailing edge swam significantly faster than the one with the symmetrical (homocercal) trailing edge, but were not significantly different from each other. When comparing two foils with the same surface area (foils 1 and 3), the one with the heterocercal shape swam ~7% faster. However, as noted by Lauder et al. (2011a), the foil with the heterocercal shape requires more energy to swim at this speed, and so the final costs of transport for the two foils are roughly equivalent. Fourth, the foil with the greatest surface area close to the actuation axis (foil 4) swims significantly faster than all other foils. This result is concordant with previous data that indicate that moving the material of the foil near the actuation axis while keeping total surface area constant can more than double swimming speeds (Lauder et al. 2011b)

Flexible flapping foils shed a vortex wake that can be compared to the wake generated by freely swimming fishes. Figure 7 shows the three-dimensional wake behind a flexible foil (like that of a bluegill sunfish, *Lepomis macrochirus*) of the same flexural stiffness as the foils shown in Fig. 6. This foil has a more realistic fish-like tail shape, and it shed a vortex wake that was similar in its general characteristics to that shown for bluegill sunfish during steady swimming: a single large vortex ring formed by the caudal fin and smaller vortical attachments produced by the dorsal and anal fins (Tytell 2006; Flammang et al. 2011a). However, the strength of the vortical connections between the wakes of the dorsal fin and caudal fin was much less than that in freely swimming bluegill sunfish (Tytell 2006; Flammang et al. 2011a).
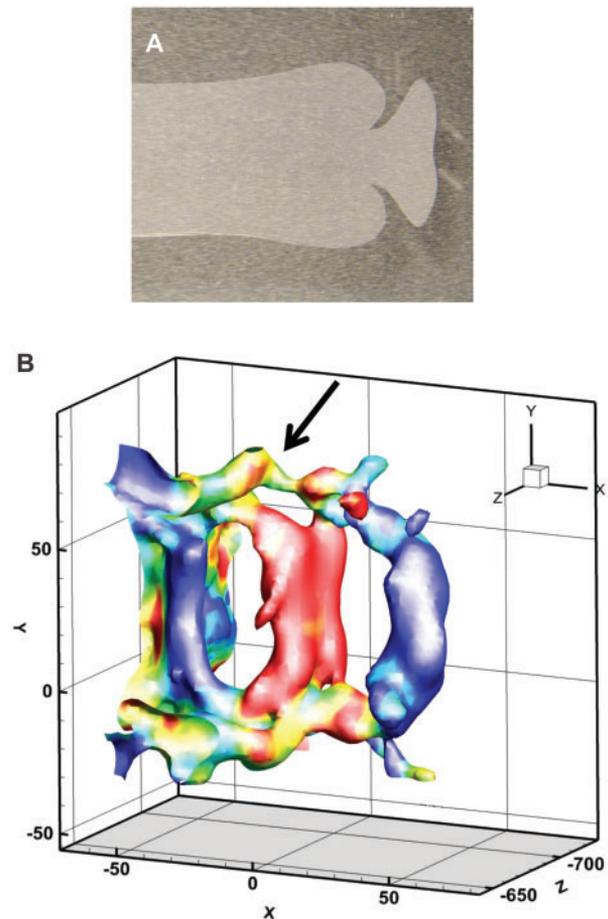

Fig. 7 Visualization of water flow patterns in the wake of the flexible foil shaped like a bluegill tail (panel A) when swimming at its self-propelled speed (material flexural stiffness = 3.1×10^{-4} Nm^2). This shape (panel A) schematically includes the trailing edges of the dorsal, anal, and caudal fins (see [Drucker and Lauder 2001; Standen and Lauder 2005]). Panel B shows patterns of flow in the wake imaged with volumetric particle image velocimetry (see text for discussion). Vortical connections between the wakes of the caudal and dorsal fins (arrow) are weak when compared to those observed in live fish. Wake vorticity is isosurfaced and then colored by Y vorticity—red is high positive (6.5 s^{-1}), blue low (1.0 s^{-1}); X, Y, and Z axes delimit the volume visualized, and units are in millimeters. (Reference to color applies to online version, not to printed black and white version.)

This may be due to the passive nature of the foil as compared to those of bluegill sunfish which actively move and stiffen the dorsal and anal fins during steady swimming (Jayne et al. 1996; Drucker and Lauder 2001; Standen and Lauder 2005). This demonstrates that fin shape alone is not a determinant of swimming hydrodynamics and that active control of fin stiffness is an important component of thrust direction and magnitude.

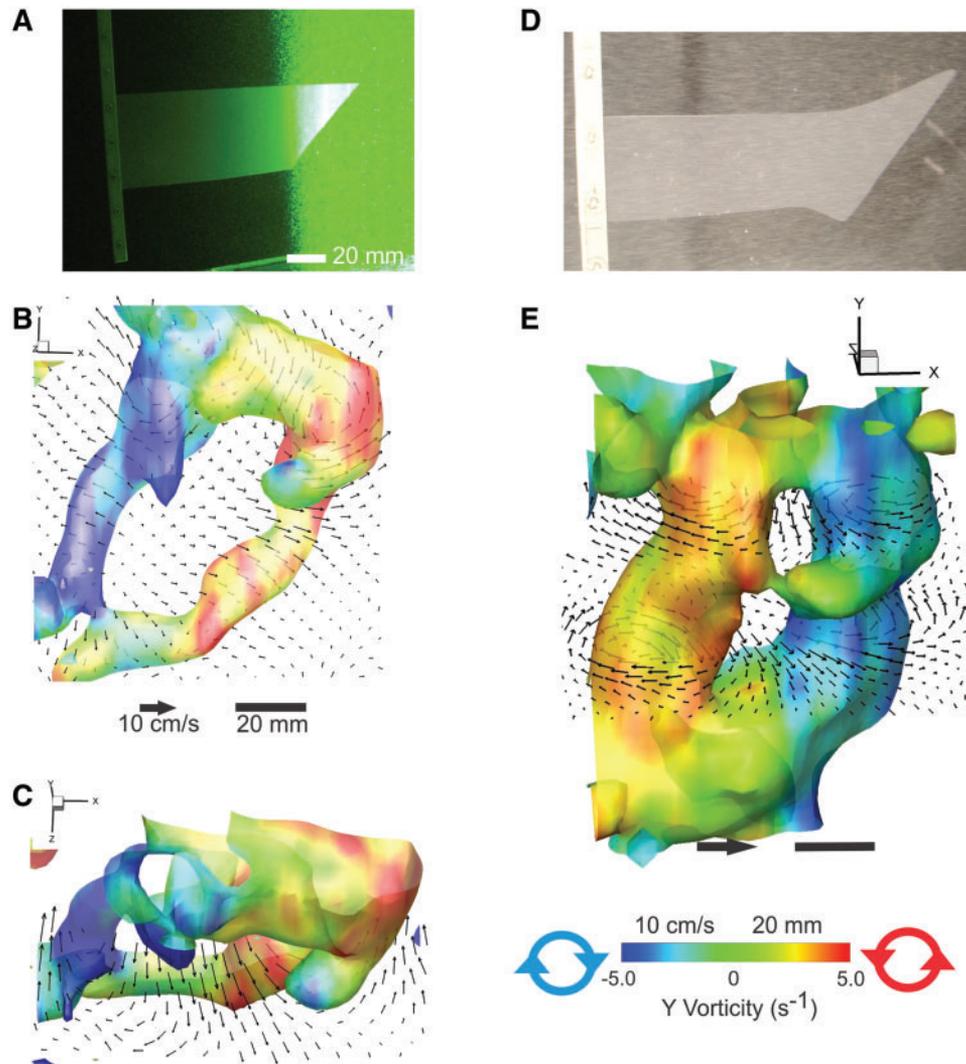Analysis of the patterns of flow in three-dimensional wakes produced by flexible foils

Fig. 8 Visualization of patterns of flow in the wake behind self-propelling flexible foils (with material flexural stiffness = 3.1×10^{-4} Nm^2) (panels A and D). These foils have an angled trailing edge that reflects the heterocercal tails of sharks either schematically (panel A) or with a somewhat more realistic shape (panel D). These foils produce a single large vortex ring, but also a weak secondary ring of lower vorticity that joins the upper portion of the large ring (panels B–E). At the values of vorticity isosurface chosen, the small weaker upper ring may not be completely closed as seen in panels B and C. Vorticity of the wake is isosurfaced and then colored by Y vorticity. Modified from Flammang et al. (2011b). (Reference to color applies to online version, not to printed black and white version.)

with angled trailing edges (Fig. 8) reveals wakes that are generally similar to those generated by swimming sharks (Wilga and Lauder 2002, 2004; Flammang et al. 2011b) with a single, large, inclined vortex ring. The secondary ring observed by Flammang et al. (2011b), however, was not observed in the wakes and instead a weak, smaller, dorsally-located ring is attached to the large vortex ring (Fig. 8). These results suggest that passive foils with inclined trailing edges are not capable of generating patterns of flow in the wake that closely mimic those of freely-swimming sharks. Instead, the highly flexible dorsal tip of the angled foils seems to generate a weak vortex ring near the top of the larger ring.

Three-dimensional analyses of the motions of foils, and particularly of the trailing edge, can assist in understanding the formation of the wake and some of its key characteristics. As seen from behind (posterior view), the lateral excursions of the symmetrical dorsal and ventral tips of tail foil 1 are equivalent at 28.0 and 28.3 mm, respectively (Fig. 9A). The asymmetrical heterocercal shape (foil 3) produced obvious asymmetries in lateral motion where the ventral tail tip only moved through a z-excursion of 21.8 mm, while the dorsal tip moved ∼50% more (42 mm; Fig. 9B) than did the homologous location on symmetrical foil 1 (Fig. 9A). This suggests that the relatively thin and pointed dorsal
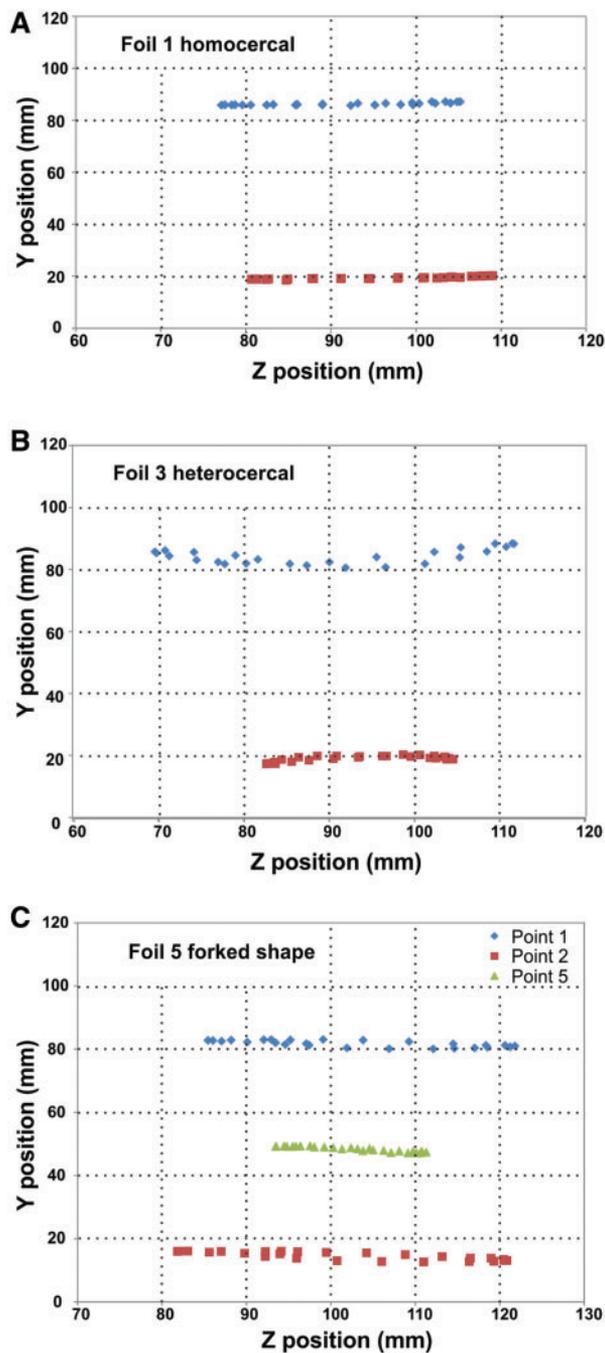
Fig. 9 Kinematics of self-propelled swimming foils (material flexural stiffness $=3.1 \times 10^{-4}$ Nm^2). Foil numbers correspond to those shown in Fig. 6. Plots show the YZ plane from posterior view, Fig. 4); point 1 is at the tip of the dorsal trailing edge, point 2 at the tip of the ventral trailing edge, and point 5 is located at the fork of foil 5. Foil 1 has similar excursions (z-axis ranges) of the dorsal and ventral tips of the tail, while the ventral margin of foil 3 undergoes much smaller excursions and both dorsal and ventral tips of this foil move in a curved trajectory, with a con-cave up and down motion, respectively. Dorsal and ventral tips of foil 5 show greater lateral excursions than do the homologous points on foil 1, while the point in the tail fork moves only half as much as the dorsal and ventral tips.

lobe of the heterocercal foil is passively flexing during lateral motion and that this motion results in larger excursions. Motion of the dorsal and ventral tail tips of the notched foil (foil 5; Fig. 9C) both underwent greater lateral excursions (mean of 37.7 mm) than did the homologous points on symmetrical foil 1, again indicating that thin passive tail regions will undergo greater lateral excursions than do homologous regions of a symmetrical tail. The center of the forked tail moves much less, with a mean excursion of 17.8 mm.

Motion of the foil viewed from lateral and ventral perspectives (Fig. 10) showed that the tips move in a figure-eight pattern in the z and x dimensions. The dorsal and ventral tail tips of symmetrical foil 1 only moved 4.35 mm in the x-direction on average, while the x-excursions of the dorsal tips of foils 3 and 5 were larger, 6.5 and 5.2 mm, respectively, indicative of passive bending (Fig. 10). The dorsal and ventral tips of forked foil 5 also moved to a greater extent than did symmetrical foil 1 in the x-dimension (mean = 5.6 mm).

Discussion and synthesis

This article has concentrated on passive flexible foils activated only at the leading edge as a model system for understanding aquatic propulsion. These passive foils have proven to be excellent models for studying locomotion of fish as they generate undulatory waves that produce thrust and self-propel at Strouhal and Reynolds numbers matching that of freely-swimming, similarly sized fish. The experimental and computational data presented here show unexpected non-linear effects of changing the length and stiffness of swimming foils, results that could not have been obtained from live fish. Additionally, the shape of the trailing edge can have significant effects on swimming speed, and analysis of tail kinematics shows that foils with an angled trailing edge swim faster. The foil with the forked tail shape exhibits the slowest swimming speeds.

However, we have also presented a number of situations in which the motion of these passive foils does not produce wake-flow patterns or kinematics that closely match those previously observed for live fishes. We suggest that these differences arise from the ability of fishes to actively stiffen the tail region using intrinsic musculature that is not represented in the passive foils. For example, Flammang (2010) recorded muscle activity from the radialis muscle, intrinsic to the heterocercal caudal fin of sharks. These data, summarized in Fig. 11, show that the radialis muscle is electrically active at the point during the
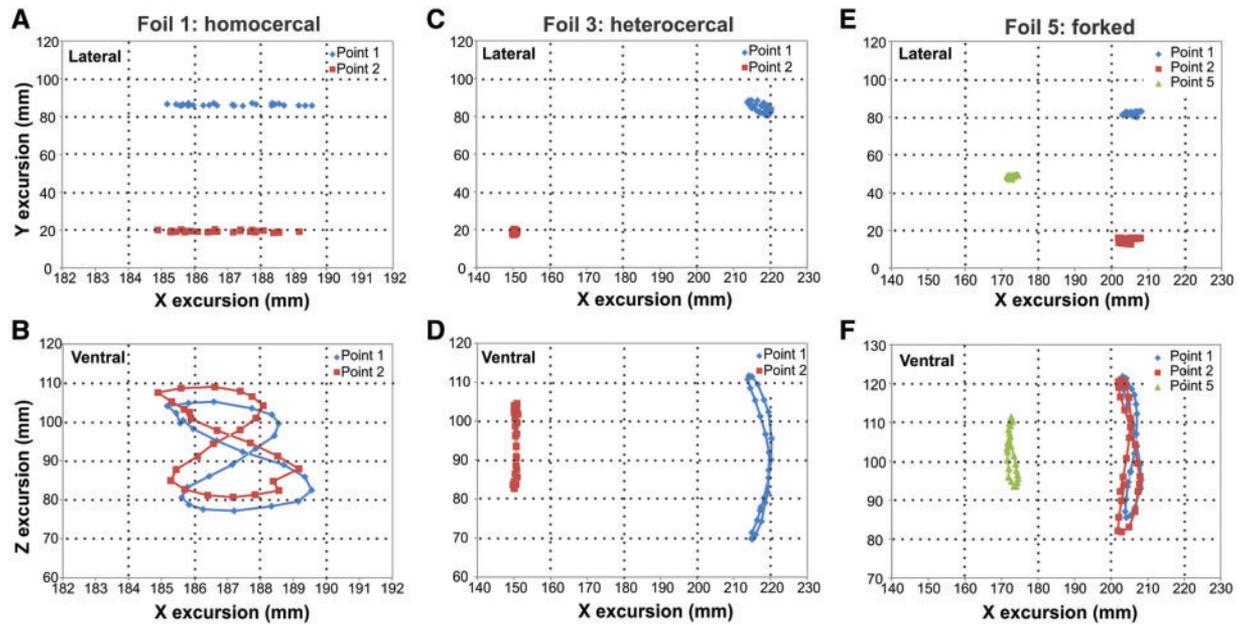
Fig. 10 Kinematics of self-propelled swimming foils (material flexural stiffness $= 3.1 \times 10^{-4}$ Nm^2). Foil numbers correspond to those shown in Fig. 6. Plots show the lateral (YX) and ventral (ZX) views, Fig. 4; point 1 is at the dorsal tail tip, point 2 at the ventral tail tip, and point 5 is located at the fork of foil 5. The points on the tips of all foils move in a figure-eight pattern, and are passively bent against oncoming flow. This is reflected in the lateral excursions of the tips of points 1 and 2. These excursions are greater for foils 3 and 5 compared to foil 1 which has a symmetrical shape (see text for further discussion).
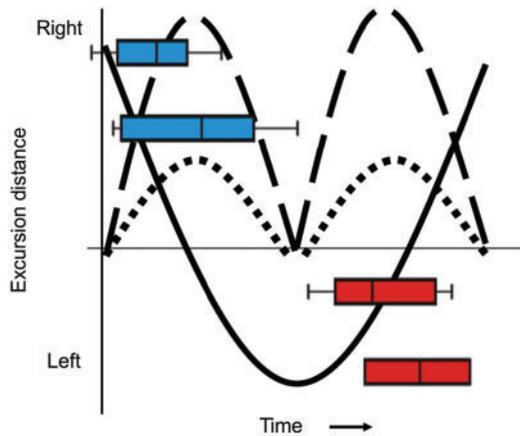

Fig. 11 Evidence of active stiffening in the tail of a freely-swimming adult spiny dogfish (*Squalus acanthias*). Plots schematically show the tail beat from one side to the other during steady swimming (solid black line), tail-beat velocity (dotted line), and drag force on the tail (large dashed line) under the simple assumption that drag is proportional to tail-velocity squared. Colored bars show measured electrical activity in the radialis muscle (intrinsic to the tail, with two electrodes in each muscle) on the right (blue) and left (red) sides. The timing of activity of the radialis muscle suggests that it acts to stiffen the tail when imposed fluid forces are highest. Error bars are ±1 SE. (Reference to color applies to online version, not to printed black and white version.)

tail beat when fluid loading on the fin is expected to be highest, and that there is considerable overlap between muscles from the right and left sides that could also stiffen the caudal fin.

Similar results were obtained for bluegill sunfish (Flammang and Lauder 2008) in which recordings of intrinsic tail muscles during steady swimming showed that these muscles actively stiffen the caudal fin. During braking and other types of maneuvering, intrinsic caudal fin musculature also controls conformation of the tail (Flammang and Lauder 2009). The extent of active control can be seen in Fig. 12, which shows a bluegill sunfish executing a braking maneuver. The dorsal and ventral lobes of the tail move to opposite sides of the body. Such control is not possible in passive foils.

Robotic models that possess active stiffening against imposed flow (Phelan et al. 2010; Tangorra et al. 2011; Esposito et al. 2012) demonstrate that the cupping behavior frequently observed in the moving fins of live fish can generate increased thrust (Tytell 2006; Lauder et al. 2007; Lauder and Madden 2007). If the passive model foils studied here could be enhanced with active stiffening elements so that the thin flexible tips were able to lead the tail in lateral motion, then we would predict enhanced thrust and increased swimming speeds. We would
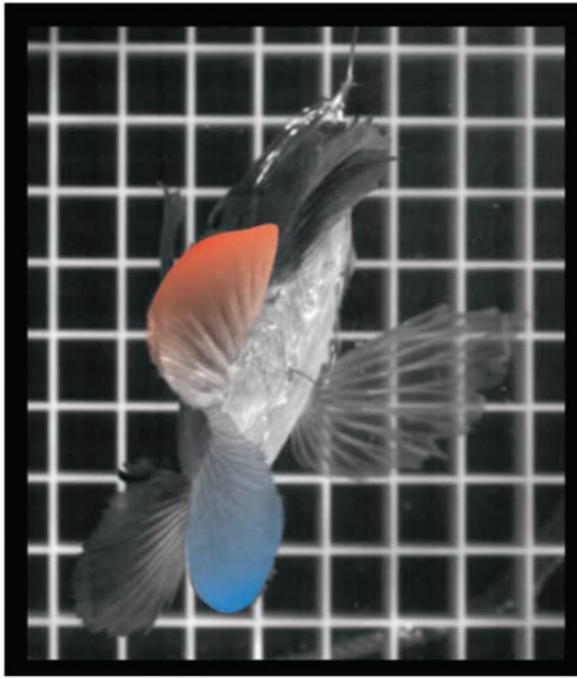
Fig. 12 Posterior view of a bluegill sunfish (*L. macrochirus*) executing a braking maneuver. This image shows active control of conformation of the tail with the dorsal lobe (red color) having moved to the upper left, and the ventral lobe (blue color) moving to the lower right. Such active control features of fish tails are not well modeled by passive foils. (Reference to color applies to online version, not to printed black and white version.)

also expect that such actively stiffened models would produce patterns of flow in the wake with more robust connections between the wakes of the dorsal, anal, and caudal fins, and that wakes of angled foils would more closely resemble those observed in live sharks.

Incorporation of the capability for stiffening that can be activated at precise phases and forces is a key challenge for the future design of simple robotic devices simulating undulatory locomotion in fishes.

References

Alben S. 2008. Optimal flexibility of a flapping appendage in an inviscid fluid. J Fluid Mech 614:355–80.

Alben S. 2009a. On the swimming of a flexible body in a vortex street. J Fluid Mech 635:27–45.

Alben S. 2009b. Simulating the dynamics of flexible bodies and vortex sheets. J Comput Phys 228:2587–603.

Alben S. 2010. Passive and active bodies in vortex-street wakes. J Fluid Mech 642:95–125.

Alben S, Baker TV, Witt C, Anderson EJ, Lauder GV. 2012. Dynamics of freely swimming flexible foils. Phys Fluids A 24:051901.

Biewener AA. 1992. Biomechanics – structures and systems. A practical approach. Oxford: Oxford University Press.

Borazjani I, Sotiropoulos F. 2010. On the role of form and kinematics on the hydrodynamics of self-propelled body/caudal fin swimming. J Exp Biol 213:89–107.

Dong H, Bozkurttas M, Mittal R, Madden P, Lauder GV. 2012. Computational modeling and analysis of the hydrodynamics of a highly deformable fish pectoral fin. J Fluid Mech 645:345–73.

Drucker EG, Lauder GV. 2001. Locomotor function of the dorsal fin in teleost fishes: experimental analysis of wake forces in sunfish. J Exp Biol 204:2943–58.

Esposito C, Tangorra J, Flammang BE, Lauder GV. 2012. A robotic fish caudal fin: effects of stiffness and motor program on locomotor performance. J Exp Biol 215:56–67.

Feder ME, Bennett AF, Burggren WW, Huey RB. 1987. New directions in ecological physiology. Cambridge: Cambridge University Press.

Felsenstein J. 2004. Inferring phylogenies. Sunderland, MA: Sinauer.

Flammang BE, Lauder GV. 2008. Speed-dependent intrinsic caudal fin muscle recruitment during steady swimming in bluegill sunfish, *Lepomis macrochirus*. J Exp Biol 211:587–98.

Flammang BE, Lauder GV. 2009. Caudal fin shape modulation and control during acceleration, braking and backing maneuvers in bluegill sunfish, *Lepomis macrochirus*. J Exp Biol 212:277–86.

Flammang BE. 2010. Functional morphology of the radialis muscle in shark tails. J Morphol 271:340–52.

Flammang BE, Lauder GV, Troolin DR, Strand T. 2011a. Volumetric imaging of fish locomotion. Biol Lett 7:695–8.

Flammang BE, Lauder GV, Troolin DR, Strand T. 2011b. Volumetric imaging of shark tail hydrodynamics reveals a three-dimensional dual-ring vortex wake structure. Proc Royal Soc London B 278:3670–8.

Garland T, Adolph SC. 1994. Why not to do 2-species comparisons: limitations on inferring adaptation. Physiol Zool 67:797–828.

Harvey PH, Pagel MD. 1991. The comparative method in evolutionary biology. Oxford: Oxford University Press.

Hedrick TL. 2008. Software techniques for two- and three-dimensional kinematic measurements of biological and biomimetic systems. Bioinsp Biomimet 3:034001.

Jayne BC, Lozada A, Lauder GV. 1996. Function of the dorsal fin in bluegill sunfish: motor patterns during four locomotor behaviors. J Morphol 228:307–26.

Kardong KV. 1998. Vertebrates. Comparative anatomy, function, evolution. 2nd ed. Dubuque (IA): W. C. Brown.

Koditschek DE, Full RJ, Buehler M. 2004. Mechanical aspects of legged locomotion control. Arthropod Struct Devel 33:251–72.

Koehl MAR, Evangelista D, Yang K. 2011. Using physical models to study the gliding performance of extinct animals. Int Comp Biol 51:1002–18.

Lauder GV. 2000. Function of the caudal fin during locomotion in fishes: kinematics, flow visualization, and evolutionary patterns. Amer Zool 40:101–22.

Lauder GV. 2006. Locomotion. The physiology of fishes. In: Evans DH, Claiborne JB, editors 3rd ed. Boca Raton (FL): CRC Press. p. 3–46.

Lauder GV, Anderson EJ, Tangorra J, Madden PGA. 2007. Fish biorobotics: kinematics and hydrodynamics of self-propulsion. J Exp Biol 210:2767–80.

Lauder GV, Lim J, Shelton R, Witt C, Anderson EJ, Tangorra J. 2011a. Robotic models for studying undulatory locomotion in fishes. Mar Technol Soc J 45:41–55.

Lauder GV, Madden PGA. 2007. Fish locomotion: kinematics and hydrodynamics of flexible foil-like fins. Exp Fluids 43:641–53.

Lauder GV, Madden PGA, Tangorra J, Anderson E, Baker TV. 2011b. Bioinspiration from fish for smart material design and function. Smart Mater Struct 20: doi:10.1088/0964-1726/20/9/094014.

Lauder GV, Tytell ED. 2006. Hydrodynamics of undulatory propulsion. Fish biomechanics. In: Shadwick RE, Lauder GV, editors. Fish physiology, Vol. 23. San Diego (CA): Academic Press. p. 425–68.

Liem KF, Bemis WE, Walker WF, Grande L. 2001. Functional anatomy of the vertebrates. An evolutionary perspective. 3rd ed. Fort Worth: Harcourt College Publishers.

Long J. 1998. Muscles, elastic energy, and the dynamics of body stiffness in swimming eels. Amer Zool 38:771–92.

Long J. 2012. Darwin's devices: what evolving robots can teach us about the history of life and the future of technology. New York: Basic Books.

Long JH, Hale M, McHenry M, Westneat M. 1996. Functions of fish skin: flexural stiffness and steady swimming of longnose gar Lepisosteus osseus. J Exp Biol 199:2139–51.

Long J, Koob-Emunds M, Sinwell B, Koob TJ. 2002. The notochord of hagfish Myxine glutinosa: visco-elastic properties and mechanical functions during steady swimming. J Exp Biol 205:3819–31.

McHenry MJ, Pell CA, Long JA. 1995. Mechanical control of swimming speed: stiffness and axial wave form in undulating fish models. J Exp Biol 198:2293–305.

Mittal R. 2004. Computational modeling in biohydrodynamics: trends, challenges, and recent advances. IEEE J Oceanic Eng 29:595–604.

Phelan C, Tangorra J, Lauder GV, Hale M. 2010. A biorobotic model of the sunfish pectoral fin for investigations of fin sensorimotor control. Bioinsp Biomimet 5:035003.

Schultz WW, Webb PW. 2002. Power requirements for swimming: do new methods resolve old questions? Int Comp Biol 42:1018–25.

Standen EM, Lauder GV. 2005. Dorsal and anal fin function in bluegill sunfish Lepomis macrochirus: three-dimensional kinematics during propulsion and maneuvering. J Exp Biol 208:2753–63.

Tangorra J, Phelan C, Esposito C, Lauder G. 2011. Use of biorobotic models of highly deformable fins for studying the mechanics and control of fin forces in fishes. Int Comp Biol 51:176–189.

Triantafyllou MS, Triantafyllou GS. 1995. An efficient swimming machine. Sci Amer 272:64–70.

Tytell ED. 2006. Median fin function in bluegill sunfish Lepomis macrochirus: streamwise vortex structure during steady swimming. J Exp Biol 209:1516–34.

Tytell ED, Borazjani I, Sotiropoulos F, Baker TV, Anderson EJ, Lauder GV. 2010. Disentangling the functional roles of morphology and motion in the swimming of fish. Int Comp Biol 50:1140–54.

Vogel S. 2003. Comparative biomechanics. Princeton (NJ): Princeton University Press.

Wainwright SA, Biggs WD, Currey JD, Gosline JM. 1976. Mechanical design in organisms. London: Edward Arnold.

Wilga CD, Lauder GV. 2002. Function of the heterocercal tail in sharks: quantitative wake dynamics during steady horizontal swimming and vertical maneuvering. J Exp Biol 205:2365–74.

Wilga CD, Lauder GV. 2004. Hydrodynamic function of the shark's tail. Nature 430:850.